



**HAL**  
open science

# Concrete creep modelling for structural applications: non-linearity, multi-axiality, hydration, temperature and drying effects

Alain Sellier, Stéphane Multon, Laurie Buffo-Lacarrière, Thierry Vidal, Xavier Bourbon, Guillaume Camps

► **To cite this version:**

Alain Sellier, Stéphane Multon, Laurie Buffo-Lacarrière, Thierry Vidal, Xavier Bourbon, et al.. Concrete creep modelling for structural applications: non-linearity, multi-axiality, hydration, temperature and drying effects. Cement and Concrete Research, 2016, 79, pp.301-315. 10.1016/j.cemconres.2015.10.001 . hal-01714901

**HAL Id: hal-01714901**

**<https://insa-toulouse.hal.science/hal-01714901v1>**

Submitted on 22 Feb 2018

**HAL** is a multi-disciplinary open access archive for the deposit and dissemination of scientific research documents, whether they are published or not. The documents may come from teaching and research institutions in France or abroad, or from public or private research centers.

L'archive ouverte pluridisciplinaire **HAL**, est destinée au dépôt et à la diffusion de documents scientifiques de niveau recherche, publiés ou non, émanant des établissements d'enseignement et de recherche français ou étrangers, des laboratoires publics ou privés.

# Concrete creep modelling for structural applications: non-linearity, multi-axiality, hydration, temperature and drying effects

Sellier Alain<sup>a,\*</sup>, Multon Stéphane<sup>a</sup>, Buffo-Lacarrière Laurie<sup>a</sup>, Vidal Thierry<sup>a</sup>,  
Bourbon Xavier<sup>b</sup>, Camps Guillaume<sup>b</sup>

<sup>a</sup>*Université de Toulouse ; UPS, INSA ; LMDC (Laboratoire Matériaux et Durabilité des  
Constructions) ; 135, avenue de Rangueil ; F-31 077 Toulouse Cedex 04, France.*

<sup>b</sup>*Andra, Direction Scientifique/Service Colis Matériaux, Parc de la Croix Blanche, 1-7 rue  
Jean Monnet, 92298 Châtenay-Malabry Cedex, France.*

---

## Abstract

Concrete creep models have to consider several important phenomena (non-linearity, multi-axiality, hydration, and thermal and drying effects) to be relevant in structural applications. A selection of experimental results of creep tests found in the scientific literature are used to highlight these phenomena. Firstly, regarding the creep rate in different directions of a specimen under various loads, it is shown that creep rate under moderate loading can derive from elastic strains. Secondly, the reason why a Drucker Prager criterion can be chosen to model non-linear creep is discussed. Thirdly the interest of resorting to a creep theory able to decouple ageing (or hydration) effects and consolidation effects is explained. Moreover, interest using a poro-mechanical formulation, in which Biot coefficient depends on stress state, to model drying creep and shrinkage is discussed in the light of short meso-scopic analysis. The effect of temperature on creep is also addressed. The numerical implementation of the proposed modelling is briefly exposed and the model responses are confronted with experimental results.

*Keywords:* Concrete, Creep, Modelling

---

\*Corresponding author

*Email address:* [alain.sellier@insa-toulouse.fr](mailto:alain.sellier@insa-toulouse.fr) (Sellier Alain)

## 1. Introduction

Long-term management of major civil engineering concrete structures such as dams, nuclear power plants, nuclear waste storage tunnels, and large bridge elements needs finite element models able to demonstrate the reliability of these structures over a long period. However, concrete is well-known to present delayed strains which control its long-term mechanical behaviour [1] [2] [3]. To consider this phenomenon, it is usual to split the total delayed strain into autogeneous shrinkage, drying shrinkage, basic creep and drying creep. The fundamental cause of delayed strains lies in the constitutive properties of hydrates [4] . The viscous property at this scale is due to instability of the bond between C-S-H sheets [5]. At larger scale, other additive non-linear phenomena could play an important role, among other effects, micro cracking of anhydrous phases and water content variation are important [1] [6] [7] [8] [9]. To model these different phenomena, a poro-mechanical framework is useful [10]; In fact poro-mechanics allows the role of water forces (capillary or disjoining) and the constitutive behaviour of solid phases to be distinguished. The objective during the model finalization was to obtain the simplest possible formulation, that was easy to implement in any structural finite element code, and able to consider the non-linearity of creep amplitude versus loading, the possible multi-axial stress states, the effects of temperature, and the effects of water, in terms of creep velocity, shrinkage and drying creep. Another requirement was to decouple the model from other non-linear aspects such as damage or plasticity, so that this formulation could be coupled with any type of non-linear model already used for structural analysis. A further preoccupation was to obtain a differential formulation able to consider the time-variation of mechanical loading or hydro-thermal conditions, while, despite this versatility, also providing an analytical solution in cases of simple loading. In a first part, the model principles are explained with reference to the physical origins of each phenomenon, then various creep tests are simulated and the numerical results are compared to experimental results. These tests concern multi-axial basic creep, uni-axial basic creep at

various loading levels, drying creep and basic creep at various temperatures and at early age. Selected in the literature for their interest and complementary, these tests can also be used for benchmarking other structural creep models or to validate their numerical implementation.

## 35 2. Constitutive equations

### 2.1. Model principles

The global scheme of the poro-mechanical model is summarized in Figure 1. It contains two branches: the left one represents the solid behaviour, with an elastic part to model instantaneous behaviour, a Kelvin module to model the reversible creep and a non-linear Maxwell module to model permanent strains. The right branch represents the effects of hydric forces (capillary pressure and variation of disjoining forces). The non-linearity of the Maxwell module means that its viscosity depends on the creep strain, corresponding to a consolidation phenomenon [11].

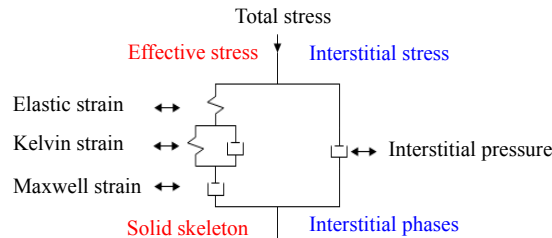


Figure 1: Idealized rheological scheme for poro-mechanical creep model

45 The model is formulated to be usable in finite element codes so as to handle the modelling of large structures. Thus, the concrete micro structure is not explicitly modelled, but the constitutive equations reflect several important underlying phenomena induced by concrete heterogeneity. First, the viscous phenomena are assumed to take place in the C-S-H inter-layer (idealized in stage 1 of figure 2), while other hydrates and aggregates are taken to be non-viscous. 50

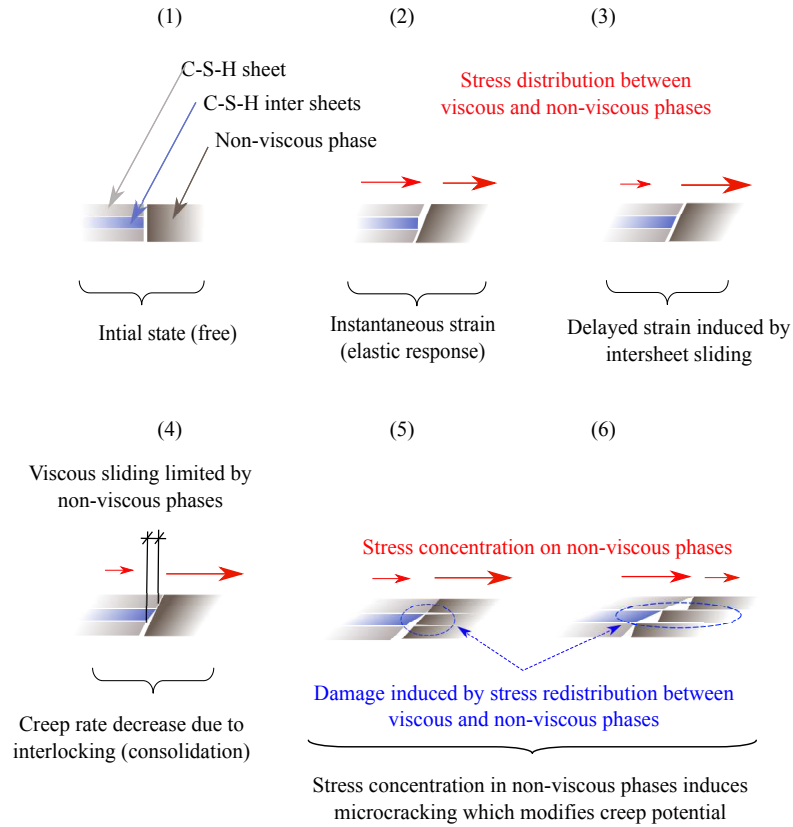


Figure 2: Idealized underlining phenomena of basic creep

When a stress is applied to the material, as symbolized by red arrows in stage (2) of figure 2, an instantaneous elastic response occurs. It is modelled by the elastic level in figure 1. However, if the stress lasts for a long time, a viscous sliding of C-S-H sheets occurs (stage (3) in figure 2). This sliding includes a reversible creep corresponding to the reversible arrangement of inter-layer water molecules [12] ; corresponding to the Kelvin module in Figure 1. It is also assumed that some inter-layer bonds can break and repair to form a new configuration (as in plasticity theory), leading to irreversible basic creep. This last strain corresponds to the non-linear Maxwell module in figure 1. When concrete is loaded, the stress in the solid skeleton transits in C-S-H and rigid

inclusions (non-viscous phase in figure 2), but, during creep, the part of the stress supported by C-S-H inter-layer is relaxed due to its viscous behaviour, leading to a stress concentration in non-viscous phases. So, the stress increases on the non viscous phases while it decreases by the same magnitude in C-S-H. As  
65 the creep velocity is proportional to the micro-stress applied to the C-S-H, this phenomenon leads to a creep velocity reduction assimilable to a consolidation process. This phenomenon can be modelled by the Kelvin module as long as the redistribution is reversible, However, as the C-S-H matrix surrounds all the other non-viscous phases, a purely viscous creep component is also possible, it  
70 is why a Maxwell module must be used to consider irreversible creep strain. Moreover, during the C-S-H matrix creep, a material rearrangement occurs, and a configuration that blocks the viscous flow can be reached (schematized by stage (4) in figure 2), where it is qualified as an interlocking phenomenon. Once the viscous flow is blocked, the stresses concentrate on the non-viscous inclusions  
75 and, if the loading level is sufficient, induce a micro structural damage (stage (5) in figure 2). This damage has been revealed experimentally by acoustic emission [8] but seems to have only negligible effects on elastic properties as illustrated in the experimental results provided in [13]. So the damage induced by creep takes place at a micro-level, it modifies the creep strain without changing the elastic  
80 modulus. When this damage occurs, as schematized in stage (6) of figure 2, it allows a new viscous flow until the next interlocking occurs on another site where non-viscous phases are not yet damaged. The relative importance of reversible creep and permanent creep depend on the proportion of elastic inclusions per unit volume of material as shown in homogenization creep models [14]. In  
85 the model presented in this paper, this fact is taken into account through the non-linearity of the Maxwell module, for which parameters can be fitted on experiments or on homogenization results.

## 2.2. *Permanent Creep*

Permanent creep corresponds to the Maxwell strain of the idealized rheological scheme 1. Permanent creep strain is assumed to derive directly from

the corresponding elastic strain components. For radial loading (no rotation of stress tensor main directions), a given eigenvalue, indexed  $I$ , of the Maxwell strain tensor can be expressed by equation (1). For the sake of simplicity, the generalization to non-radial loading will be given at the end of the present section. In equation (1) the creep velocity is assumed to be proportional to the corresponding elastic components  $\varepsilon_I^E$ . The proportionality between the creep velocity and the elastic strain is supported by experimental evidence showing that multiaxial creep starts with relative strain velocities in different directions ( $I$ ) proportional to the elastic strains as shown in Gopolkrishnan et al.'s [15] or Kim et al.'s [16] works. This assumption is successfully confronted with several experimental results in the second part of the present paper.

$$\frac{\partial \varepsilon_I^M}{\partial t} = \frac{\varepsilon_I^E}{\tau_I^M} \quad (1)$$

In this equation  $\tau_I^M$  is a characteristic time associated with the Maxwell strain component  $\varepsilon_I^M$ , with  $I$  corresponding to eigen-directions of the Maxwell strain tensor.  $\tau_I^M$  is defined by equation 2.

$$\tau_I^M = \tau_{ref}^M C_I^C \quad (2)$$

The characteristic time is split into  $\tau_{ref}^M$  a reference characteristic time characterizing the initial material state and  $C_I^C$  a consolidation function expressing the consolidation state. The reference characteristic time,  $\tau_{ref}^M$ , is a fitting parameter that is inversely proportional to the initial creep velocity measured in reference conditions (high humidity, reference temperature, given loading rate without previous creep strain). The consolidation function  $C_I^C$  was initially introduced as an increasing function of the Maxwell strain normalized by a constant strain called *creep potential* in [11]; it was improved in [17] to consider the non-linear dependence of this creep potential on the loading rate. The interest of the present new version resides, in particular, in its anisotropic formulation which allows different consolidation velocities to be considered in the three main directions of creep. As shown in the application section, this formulation is able to consider, with a smaller number of parameters, a more complex loading pass

or loading chronology than in previous models. Its expression is given by (3). The objective of the consolidation function is to consider the decrease of creep strain velocity with time without resorting explicitly to the time variable, which is not a state variable and could lead to confusion between consolidation and the consequences of hydration. In fact, creep rate reduction by consolidation and hydration have different physical origins and care must be taken to treat them separately in creep models.

$$C_I^C = \frac{1}{k} \exp \left( \frac{1}{k} \left( \frac{\varepsilon_I^M}{\varepsilon_I^E} \right)^+ \right) \quad (3)$$

The positive part  $()^+$  means that the consolidation coefficient cannot be smaller than  $1/k$ .  $\varepsilon_I^E$  is the elastic normal strain in direction I, (subscript I is relative to a main direction of the permanent creep strain tensor). The form chosen for the consolidation coefficient is such that when  $\varepsilon_I^M \gg k\varepsilon_I^E$  the characteristic time increases, which in turn slows the creep velocity.  $k$  is the creep coefficient for the current temperature,  $T$ , humidity,  $H$  and loading,  $M$ . When the  $THM$  conditions are constant the model has an analytical solution that allows the role of  $k$  and  $\tau_{ref}^M$  to be easily understood. The analytical solution corresponding to uniaxial, and constant loading is given by equation (4).

$$\varphi^M(t) = k \ln \left( 1 + \frac{t}{\tau_{ref}^M} \right) \quad (4)$$

with  $\varphi^M(t)$  the permanent basic creep function :

$$\varphi^M(t) = \frac{\varepsilon_{test}^M}{\varepsilon_{test}^E} \quad (5)$$

where  $\varepsilon_{test}^E = \sigma_{test}/E$  is the elastic strain under the applied stress  $\sigma_{test}$ , and  $E$  is the Young's modulus. An illustration of influential parameters is given in Figure 3. Equation (4) and Figure 3 show that the initial specific permanent creep velocity is  $k/\tau_{ref}^M$ , that  $\tau_{ref}^M$  allows to the creep curve to be shifted along time axes, while  $k$  changes the specific creep amplitude.

*Influence of environmental conditions* . At nano-scale, basic creep is believed to be caused by atomic link instabilities, which are themselves affected by physical

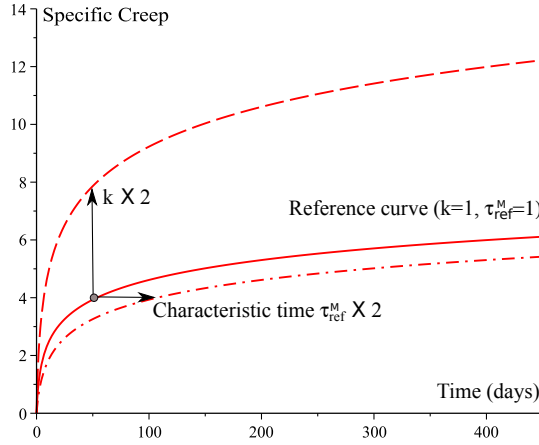


Figure 3: Specific Creep from Maxwell module, parametric study with  $k_{ref}$  and characteristic time  $\tau_{ref}^M$

conditions (temperature (T), Humidity (H) and mechanical loading (M) [18]). At larger scales (micro and meso-scale) stress redistribution between viscous phases and non-viscous phases leads to consolidation and damage, as schematized in figure 2. Consequently, the creep velocity is managed by three physical

100 conditions:

- Temperature (T),
- Humidity (H),
- Mechanical loading (M).

The *THM* conditions act on creep velocity through three multiplicative functions,  $C^T$ ,  $C^H$  and  $C^M$ , affecting  $k$  ( which controls the creep amplitude as illustrated in figure 3).

$$k = k_{ref} C^T C^H C^M \quad (6)$$

In (6),  $k_{ref}$  is the reference creep coefficient defined as the ratio of a characteristic strain  $\varepsilon_{ref}^M$  to a conventional characteristic elastic strain  $\varepsilon_{ref}^E$ .

$$k_{ref} = \frac{\varepsilon_{ref}^M}{\varepsilon_{ref}^E} \quad (7)$$

In (7),  $\varepsilon_{ref}^M$  is the fitting parameter called the *reference creep potential*, because the creep function amplitude is proportional to  $\varepsilon_{ref}^M$ . As the creep amplitude depends on the loading level,  $\varepsilon_{ref}^M$  is defined for a given loading level corresponding to the elastic strain  $\varepsilon_{ref}^E$ . As  $\varepsilon_{ref}^E$  and the reference creep potential  $\varepsilon_{ref}^M$  are then linked,  $\varepsilon_{ref}^E$  is called the reference elastic strain, as a remember that it is the elastic strain corresponding to the loading level used to define  $\varepsilon_{ref}^M$ .

In equation (6),  $C^T$  accounts for the influence of temperature on creep potential,  $C^H$  the influence of humidity, and  $C^M$  the non-linear effect of mechanical loading, since the linear dependence of creep amplitude on loading is already considered in equation (1) by the elastic strain.

**Water effect on basic creep** C-S-H interlayer cohesion and disjoining forces are sensitive to the water saturation degree as explained in [1], or at lower scale, in [9] and [18]. In a structural model, as suggested in [19], only a macroscopic approximation of these complex underlying phenomena can be envisioned. An ad hoc linear approximation is used to consider the reduction of creep velocity when concrete is dry:

$$C^H = S_r \quad (8)$$

with  $S_r = \phi_w/\phi$  the liquid water saturation rate of the porosity ( $\phi_w$  is the volume water content and  $\phi$  the total volume of porosity). The higher the water saturation  $S_r$ , the higher the specific creep amplitude. Note that the simple relation (8) is not the only effect of water on delayed strain. The section concerning the effects of hydric forces (22) focuses on the consequences of drying on delayed strains and proposes a method to model drying shrinkage and the Pickett effect in a unified poro-mechanical approach.

**Temperature effects on basic creep** Temperature has two effects on basic creep: On one hand, it modifies the intrinsic viscosity of viscous phases containing free water, due to the dependence of water viscosity on temperature, and, on the other hand it causes differential dilation between phases. This can increase creep potential by releasing viscous phases, and cause thermal damage [20, 21]. So the temperature function affecting the characteristic time (2) is expressed as the product of two functions  $C_w^T$  and  $C_p^T$  which consider the effect of temperature on viscosity and creep potential respectively.

$$C^T = C_w^T C_p^T \quad (9)$$

As shown in [22],  $C_w^T$  can be taken equal to the water viscosity dependence on temperature; it is an Arrhenius law independent of the material composition. In (10)  $E_w^a \approx 17000 J/mol$  is the activation energy of water viscosity,  $T_{ref}$  is the reference temperature for which the characteristic time  $\tau_{ref}^M$  is fitted, and  $R = 8.31 J/mol/K$  the gas constant.

$$C_w^T = \exp\left(-\frac{E_w^a}{R}\left(\frac{1}{T} - \frac{1}{T_{ref}}\right)\right) \quad (10)$$

$$C_p^T = \begin{cases} \exp\left(-\frac{E_p^a}{R}\left(\frac{1}{T} - \frac{1}{T_{thr}}\right)\right) & \text{if } T > T_{thr} \\ 1 & \text{if } T \leq T_{thr} \end{cases} \quad (11)$$

$C_p^T$  depends on the material composition through two fitting parameters:  $E_p^a \approx 25000 J/mol$  and  $T_{thr} \approx 45^\circ C$  the threshold temperature from which thermal damage appears and modifies the creep potential according to [20] (as illustrated in figure 19).

**Non-linear effect of mechanical loading on basic creep** Coefficient  $C^M$  considers the possible non-linear dependence of creep potential on mechanical loading level. So,  $C^M$  starts from 1 for weakly loaded material and diverges if the loading level reaches a critical value causing tertiary creep. Tertiary creep is believed to occur only in cases of micro-structure damage as schematized in Figure 2 (stage 6), An ad hoc *creep damage criterion* is introduced. Several criteria have been tested, and the best results were obtained with a Drucker Prager

criterion form [23]. So,  $C^M$  (12) depends on the loading level only through the equivalent Drucker Prager shear stress  $\tau^{DP}$  (13). This choice is justified in the application section below, where creep rates under deviatoric stress states (figures 13 or 21 ) are compared to creep under an isotropic stress state (Figure 15).

$$C^M = \frac{\tau_{cr}^{DP}}{\tau_{cr}^{DP} - \tau^{DP}} \text{ with } \tau^{DP} < \tau_{cr}^{DP} \quad (12)$$

In (12),  $\tau_{cr}^{DP}$  is the critical stress leading to tertiary creep. The Drucker Prager

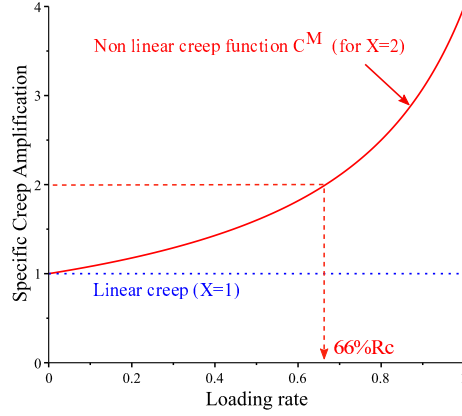


Figure 4: Specific creep amplification function  $C^M$  versus loading rate; x stands for  $\chi^M$  cf. equation (15)

equivalent stress  $\tau^{DP}$  corresponds to expression 13. This expression, often used in plasticity and visco-plasticity models [24, 25, 26, 27], is able to consider the benefits of triaxial confinement in reducing impact of deviatoric stresses in terms of damage.  $\tau^{DP}$  (13) considers the two first stress tensor invariants:

$$\tau^{DP} = \sqrt{\frac{\sigma^d : \sigma^d}{2}} + \delta \frac{\text{Tr}(\sigma)}{3} \quad (13)$$

In (13)  $\delta$  is the confinement effect coefficient which takes the effect of hydrostatic pressure ( $-\text{Tr}(\sigma)/3$ ) on shear strength into account.  $\sigma^d$  is the deviatoric part of the stresses tensor. The critical stress leading to tertiary creep ( $\tau_{cr}^{DP}$  in equation (12)) can be linked to the corresponding uniaxial critical stress

intensity  $\sigma_{cr}$ . The relation involves the confinement coefficient  $\delta$  and assumes that the uniaxial critical stress is a compression.

$$\tau_{cr}^{DP} = \frac{\sigma_{cr}}{\sqrt{3}} \left( 1 - \frac{\delta}{\sqrt{3}} \right) \quad (14)$$

To facilitate fitting,  $\sigma_{cr}$  is computed from a non-linear amplification coefficient  $\chi^M$ , supplied by the user and corresponding to the non-linearity of creep under a conventional applied compression stress of  $66\%R_c$  as illustrated in figure 4. With this definition, the link between  $\chi^M$  and  $\sigma_{cr}$  is :

$$\sigma_{cr} = \frac{2}{3} \left( \frac{\chi^M}{\chi^M - 1} \right) R_c \quad (15)$$

To illustrate the effect of  $\chi^M$ , in Figure 4 a value of  $\chi^M = 2$  was used to plot the red curve. It can be noted that specific creep is then multiplied by 2 under  $66\%R_c$  ( $R_c$  is the uniaxial compressive strength), comparatively to the 140 dotted blue line corresponding to  $\chi^M = 1$  for which the specific creep remains independent of the applied stress.

*Non-radial loading case.* Equation (1) is applicable only in cases of radial loading. Its generalization to non-radial loading leads us to consider cases for which the current main directions of Maxwell strains tensor are different from the main directions of elastic strains tensor. In such cases, it is proposed to assess the characteristic times in the main direction of the Maxwell strain tensor (directions  $I$  or  $J$  in equation (17)), and to choose the minimal characteristic time for extra-diagonal components as expressed by equation (16). This choice can be justified by the fact that, as shear stress has to verify the symmetry condition of the stress tensor, it is limited by the weakest viscosity between directions  $I$  and  $J$ , which corresponds to the lower characteristic time condition in equation (16).

$$\tau_{IJ}^M = \min(\tau_I^M, \tau_J^M) \quad (16)$$

Relationship (1) can then be generalized as follows:

$$\frac{\partial \varepsilon_{IJ}^M}{\partial t} = \frac{\varepsilon_{IJ}^E}{\tau_{IJ}^M} \quad (17)$$

The fact that two subscripts  $I$  and  $J$  subsist in (17) means that the relation is given in the principal base of Maxwell strains, where the elastic strain tensor is projected for the computation of creep velocity. Once the creep velocities have been computed for each component  $IJ = [11, 22, 33, 12, 13, 23]$ , the Maxwell strain increment is deduced and returned in the fixed base where it can be added to the previous Maxwell strain tensor.

### 2.3. Reversible creep

Reversible creep is modelled using a Kelvin module (see Figure 1) in which the asymptotic strain is assumed to be proportional to the elastic strain. Thus the final amplitude of reversible creep is  $\varepsilon_{ij}^E/\psi^K$ . Subscripts  $ij$  correspond to the base in which the stress tensor is expressed. In equation (18),  $\tau^K$  is the characteristic time.

$$\frac{\partial \varepsilon_{ij}^K}{\partial t} = \frac{1}{\tau^K} \left( \frac{\varepsilon_{ij}^E}{\psi^K} - \varepsilon_{ij}^K \right) \quad (18)$$

Reversible creep, like permanent creep, depends on temperature and water content. The same coefficients,  $C_w^T$  (equation 10) and  $C^H$  (equation 8), as for permanent creep are used to create a dependence of reversible creep velocity on environmental conditions. Coefficients  $C_p^T$  and  $C^M$  are not used in the Kelvin module. This means that the kinetics of reversible specific creep is modified but its amplitude is not.

$$\tau^K = \tau_{ref}^K C_w^T C^H \quad (19)$$

To fit  $\psi^K$  and  $\tau_{ref}^K$  a creep test with strain recovery is needed. As shown in the Application section of the present paper (Figures 13, 21), the Kelvin strain usually represents about 20 to 25% of the elastic strain. Therefore it corresponds to a coefficient  $\psi^K$  close to 4 or 5 (see fitting in table 4).

### 2.4. Shrinkage and drying creep

Water has complex effects in porous media. It can react with the solid skeleton, be adsorbed on porous walls, and exert capillary and disjoining forces on the solid skeleton. In some materials, such as clay or concrete, water molecules

are present in nanoscopic inter-sheets, causing attractive or repulsive forces according to their environmental conditions (mechanical loading, temperature and relative humidity)[18] [7]. These effects have several macroscopic consequences. To model the most important macroscopic consequences of water solid interactions, it is convenient to resort to the Biot theory in the context of poromechanics (Biot theory has been extended to non saturated media by Coussy [28]). In fact the water capillary pressure, for example, exerts a tension perpendicular to the pore walls, which is balanced by orthogonal compression forces, parallel to the pore walls, causing shrinkage. Although capillary forces exist mainly at high humidity, other forces, like disjoining force variations can have similar consequences on drying cement pastes. In any case, as these forces reside in the cement paste, the paste shrinks and causes a heterogeneous stress field at the micro and meso-scope scales. The way the hydric force effects are considered in the present model, is in relation with the possible damage induced by this stress field heterogeneity. To understand the formulation, a simplified mesoscopic analysis, illustrated in figure 5, is used. In figure 5, two configurations are envisioned. On the left side (1), concrete is free of applied stress, the hydric forces effects are simulated by an imposed shrinkage within the paste. It can be observed that interfaces between paste and aggregates are in tension, which can cause paste-aggregate debonding. These breaks, when they occur, limit transmission of forces induced by the paste shrinkage to larger scale. The corresponding meso-scope cracks have been confirmed experimentally, for example by micro-tomography in [29]. In contrast, on the right side (2) of Figure 5, a vertical compression is applied to the concrete. It can be observed that the combination of external compression loading and paste shrinkage leads to tensile stresses only in directions orthogonal to the compression (on average), while, vertically, the interface between paste and inclusions stays in compression and cannot break. Consequently the forces induced by paste shrinkage continue to be transmitted in this direction, amplifying the macroscopic shrinkage, comparatively to the free case. This phenomenon is considered in the model through a modulation of the Biot coefficient in unsaturated conditions.

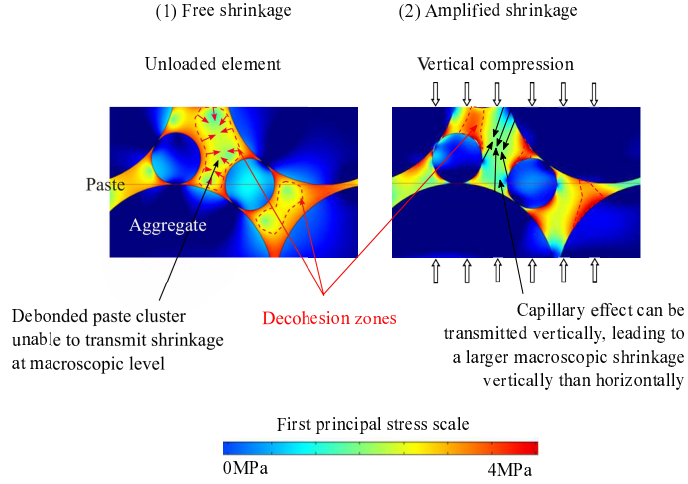


Figure 5: Stress field heterogeneity at meso-scale and consequences in terms of shrinkage forces transmission to macroscopic scale

*Interactions between water and solid.* For sake of simplicity, the different effects of water forces (disjoining and capillary) are merged into a single *equivalent capillary pressure*. As illustrated above, the efficiency of action of the equivalent capillary pressure depends on the stress state  $\sigma$ . If damage occurs, it limits the equivalent capillary pressure transmission from paste to other phases and the macroscopic effect of paste shrinkage is reduced. Conversely, if a compression stress is applied, damage induced by differential shrinkage between paste and aggregate is avoided in the direction of application of stress, and the capillary pressure effect is better transmitted. In the poromechanical theory, the efficiency of transmission of hydric forces from paste to the macro scale is managed by the Biot coefficients ( $b$  and  $M_{shr}$  in the following). Thus, change in the hydric force transmission quality can be considered through a modification of the Biot coefficients. To consider this non-linear interaction between solid skeleton and water effects during drying or humidification as simply as possible, the poromechanical formulation of the total stress  $\sigma$  is written in an incremental form, in which the Biot coefficients depend on the stress state. The corresponding equation (20), which exists only for normal stresses, is expressed in the main

direction of total stresses. The incremental formulation allows the current stress state to be considered as not acting on the total hydric forces but only on their increments. This means that, if a material was dried under a given applied stress, unloading after drying will not change the shrinkage amplitude.

$$\frac{\partial \sigma_I}{\partial t} = \frac{\partial \sigma'_I}{\partial t} + \frac{\partial(b_w p_w)}{\partial t} \left( 1 + \frac{|\sigma_I|}{\sigma_{dc}} \right) \quad (20)$$

with  $\sigma_{dc}$  a fitting parameter such that the equivalent capillary pressure effects are doubled when the material is subjected to a compression  $\sigma_I = -\sigma_{dc}$ .  $\sigma_I$  is a principal stress.  $\sigma_{IJ}$  and  $\sigma'_{IJ}$  are respectively the total and effective stress expressed in the principal base of total stresses.  $b_w p_w$  is the equivalent capillary pressure effect on the material in accordance with the poro-mechanical theory [28], with  $b_w$  the Biot coefficient of unsaturated media equal to the Biot coefficient in saturated condition  $b$  modified by the saturation rate,  $S_r$ :

$$b_w = b \cdot S_r \quad (21)$$

How the interaction between capillary pressure ( $p_w$ ), Biot coefficient ( $b_w$ ), and stress state ( $\sigma$ ), takes place when  $\sigma_I$  is a tensile stress has not been fully clarified experimentally. But, as an induced tensile shrinkage is mentioned in the literature [30], the proposed relation is kept also in tension where it amplifies the shrinkage increment proportionally to the tensile stress. In this case, according to [8], the physical origin could be a self dessication induced by a diffuse micro cracking able to restart hydration processes. In any case, in the present model, this aspect remains approximately considered by the linear dependence of the shrinkage increment to the stress, and, certainly, could be improved under the light of appropriate experiments.

*Equivalent Capillary Pressure.* The equivalent capillary pressure can be modelled using the two-parameters equation known as the *Van-Genuchten model* [31]. This equation provides the equivalent capillary pressure as a function of the saturation rate ( $S_r$ ). If gas pressure is negligible relative to water pressure ( $p_w$ ), the water pressure can be directly expressed as a function of the water

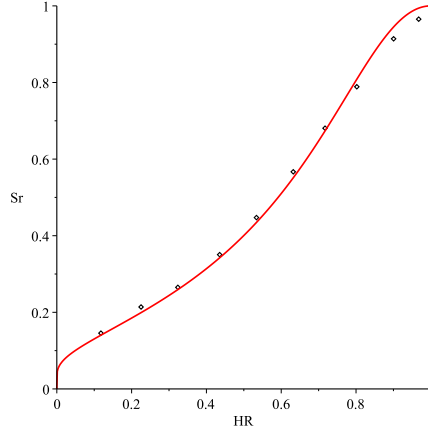


Figure 6: Isotherm (dots: experiments from [32], line: Van Genuchten equation with  $M_{shr} = 41MPa$  and  $m_{vg} = 0.5$ )

saturation rate (22) as illustrated in figure 6.

$$p_w = -M_{shr} \left( S_r^{\left(-\frac{1}{m_{vg}}\right)} - 1 \right)^{(1-m_{vg})} \quad (22)$$

In equation (22),  $M_{shr}$  and  $m_{vg}$  are fitting parameters controlling the shape of the water retention curve, as illustrated in figure 6.

### 2.5. Hydration

As the creep rates derive from elastic strains in the model, the hydration can be considered by simply using elastic properties depending on the hydration degree. For this purpose, the de Schutter's [33] equation form (23) is adopted to consider the effect of hydration on mechanical properties. Mechanical properties then depends on the hydration rate  $\xi$  as follows :

$$\frac{X}{X_{ref}} = \begin{cases} 0 & \text{if } 0 \leq \xi \leq \xi_{thr} \\ \left( \frac{\xi - \xi_{thr}}{\xi_{ref} - \xi_{thr}} \right)^n & \text{if } \xi > \xi_{thr} \text{ with } \xi < 1 \end{cases} \quad (23)$$

In(23),  $X_{ref}$  is the mechanical property for the material hydrated at  $(\xi_{ref})$ ,  $\xi_{thr}$  is the hydration threshold corresponding to the concrete solidification [34],

205 which depends mainly on the aggregate content, and varies from 0.1 for concrete  
 until to 0.3 for cement paste.  $n$  is the non-linearity coefficient. The fact that  $n$   
 is not equal to the unit for the Young modulus means that the contribution of  
 the hydrates created close to the  $\xi_{thr}$  is different then hydrates created later.  
 As the Creep velocity depends on the elastic strain (1), and thus to the Young  
 modulus, this implies that early age hydrates have a different contribution on  
 210 creep velocity than delayed hydrates . Usual values of  $n$  and  $\xi_{thr}$  are given in  
 table 1. As shown in the applications section, the fact that creep strains derive

Table 1: Usual data for De Schutter evolution law

Parameter	$X$ in (23)	$n$
Young's modulus	$E$	0.66
Compressive strength	$R_c$	1
Shrinkage modulus	$M_{shr}$	1
Biot coefficient	$b$	1

from elastic strains, which themselves depend on hydration degree though the  
 elastic properties, is sufficient to explain faster creep at early age. An illustration  
 of the efficiency of this method is given in [35]. In this paper, an experiment  
 215 is carried out with a concrete cylinder, 60 cm high, 80 cm diameter, to test  
 the ability of the model to simulate the behavior of concrete since casting. The  
 evolutions of temperature and strain versus time are computed by the model and  
 compared with success to the experimental results. For the sake of simplicity,  
 the creep parameters can be kept independent of the hydration degree, (only  
 220  $E$ ,  $R_c$ ,  $M_{shr}$ ,  $b$  depend on the hydration degree). However, to consider the  
 effects of hydration on the material state, two compatibility conditions have to  
 be added: First, the internal variables have to be actualized to take account  
 of the possibility of self healing during hydration as explained in [36]. In a  
 similar way, the stress state in the elastic and Kelvin elastic branches (see figure  
 225 1) have to remain compatible with the hydration degree during its evolution.  
 This implies a reduction of the elastic and Kelvin strains, which then have to

be considered as internal variables (24). Equation set (24) allows the elastic strain to be reduced according to the evolution of the hydration degree . This updating has an important consequence on the reversible creep module, since, in equation (18), the reversible creep depends on the elastic strain.

$$\forall(i,j) \begin{cases} \frac{\partial S_{ijkl}}{\partial \xi} \varepsilon_{kl}^E + S_{ijkl} \frac{\partial \varepsilon_{kl}^E}{\partial \xi} = 0 \\ \frac{\partial S_{ijkl}}{\partial \xi} \varepsilon_{kl}^K + S_{ijkl} \frac{\partial \varepsilon_{kl}^K}{\partial \xi} = 0 \end{cases} \quad (24)$$

With  $S_{ijkl}$  the stiffness matrix computed with  $E(\xi)$  .

## 2.6. Numerical implementation

Differential equations (1) and (18) can be time discretized using a classical semi-implicit Euler scheme (also called  $\theta$  method). A set of equations involving the six Kelvin strain components and six Maxwell components is formed, to be solved at each time step increment (25).

$$\forall(i,j) \begin{cases} \Delta \varepsilon_{ij}^K \left( 1 + \frac{\theta \Delta t}{\tau^K} \left( 1 + \frac{1}{\psi^K} \right) \right) + \frac{\theta \Delta t}{\tau^K \psi^K} \Delta \varepsilon_{ij}^M = \frac{\theta \Delta t}{\tau^K \psi^K} \Delta \varepsilon_{ij} + \frac{\Delta t}{\tau^K} \left( \frac{\varepsilon_{ij}^E}{\psi^K} - \varepsilon_{i,j}^K \right) \\ \Delta \varepsilon_{ij}^M \left( 1 + \frac{\theta \Delta t}{\tau_{ij}^M} \right) + \Delta \varepsilon_{ij}^K \frac{\theta \Delta t}{\tau_{ij}^M} = \frac{\Delta t}{\tau_{ij}^M} \varepsilon_{ij}^E + \frac{\theta \Delta t}{\tau_{ij}^M} \Delta \varepsilon_{ij} \end{cases} \quad (25)$$

In (25),  $\Delta t$  is the time step and  $\theta$  the semi implicit coefficient, taken equal to 1/2 to obtain a mid point method. In these equations, total strains ( $\varepsilon_{ij}^K, \varepsilon_{ij}^M, \varepsilon_{ij}$ ) are defined at the beginning of the time increment, while strain increments ( $\Delta \varepsilon_{ij}^K, \Delta \varepsilon_{ij}^M$ ) are the unknowns for the current time step and  $\Delta \varepsilon_{ij}$  is the imposed strain increment. Variations of  $\tau_{ij}^M$ , due to consolidation and variations in environmental conditions, are taken into account explicitly by actualizing consolidation coefficients (3) at the end of the time step, ready for the next one. This approximation is admissible when relative variations of characteristic time are slow enough. Otherwise the consolidation coefficient can be linearized to improve the convergence rate. In any case, the time step  $\Delta t$  can be limited to avoid inaccuracy induced by a possible inadequate choice of time step by user. Criteria

usable to control the time step increment can be deduced from characteristic times. For example, the condition  $\Delta t \leq \min(\zeta\tau_{ij}^M, \zeta\tau^K/(1 - \varepsilon^E/\psi^K/\varepsilon^K))$  is
   
 250 currently used in the model with  $\zeta = 10\%$ . This means that, if the asymptotic strain of the Kelvin module is not reached, the time step is chosen to avoid strain increments greater than 10% of remaining Kelvin strain, without exceeding 10% of the Maxwell characteristic time. *As the Kelvin module strain is generally reached a few days after loading, the time step is then controlled by*
  
 255 *the Maxwell characteristic time, which increases with the consolidation coefficient. Thank to this method the time step can be more and more large, and the calculus more and more rapid. If the user chooses arbitrarily a time step too large, the program cut the imposed time step in these optimal sub-steps and assume a linear variation of the hydration degree from a time sub-step to the next.*
  
 260 *This method allows to compute finite elements models with several thousand nodes in a reasonable time as illustrated in [37] or [38]. More accurate criteria to choose the optimal time step could certainly be derived from equations set (25), but the proposed one has been used with success by the authors. It constitutes a good compromise between the computational cost for the optimal*
  
 265 *time step assessment and the time spent for the creep calculus itself. The algorithm is finally relatively robust because even if the criterion of  $\zeta = 10\%$  used to choose the optimal time step is larger, the error on creep strain assessment during an increment leads to a larger consolidation at the end of the time step, which in return reduces the creep velocity for the next increment. There is an*
  
 270 *auto-compensation of too large time steps by the consolidation function. This phenomenon is certainly the principal reason of the robustness of the algorithm.*

### 3. Applications

The previous equations were implemented in the finite element code **CAST3M (CEA)** [39] and are currently being implemented to improve an existing chemo-
   
 275 mechanical model [40] implemented in **CODE ASTER (EDF)**. This part presents the applications to several experimentations taken from the literature in order

to validate the ability of the model to simulate:

- basic creep under uniaxial and multiaxial loading in compression (test by Kim and by Gopalakrishnan),
- 280 • basic creep and autogeneous shrinkage at early age (tests by Buffo-Lacarriere)
- basic creep at different temperature levels (tests by Ladaoui),
- drying creep (tests by Granger),
- creep non-linearity (test by Roll).

For each part, the conditions of the experimentation (mix-design, instantaneous characteristics) are given in Tables 2 and 3. The model parameters necessary to reproduce the behaviour, calibrated on experimental data, are summed up in Table 4.

Table 2: Mix-design (C: cement proportion in  $kg/m^3$ , W/C: water cement ratio)

Material	Reference	C	W/C
CI	Kim, 2005 [16]	320.	0.58
CII	Kim, 2005 [16]	418.	0.40
CIII	Kim, 2005 [16]	506.	0.32
	Gopalakrishnan, 1969 [15]	260.	0.72
	Ladaoui, 2011 [22]	400.	0.45
	Granger, 1996 [41]	350.	0.54
	Roll, 1964 [13]	300.	0.52
Mortar	Buffo-Lacarriere, 2011 [36] [42]	489.	0.60

### 3.1. Basic creep under uniaxial loading in compression

The Experimental and calculated strains obtained on uniaxial basic creep tests in compression (Kim) have been plotted in Figures 7, 8 and 9 for each concrete mix-design (concrete CI with a compressive strength of 26 MPa in 7,

Table 3: Instantaneous characteristics of concrete ( $R_c$ : compressive strength,  $R_t$ : tensile strength,  $E$ : Youngs modulus,  $\nu$  : Poisson ratio)

Material	reference	$R_c$ (MPa)	$R_t$ (MPa)	$E$ (MPa)	$\nu$
CI	Kim, 2005	26.	-	24,010	0.18
CII	Kim, 2005	44.1	-	29,841	0.18
CIII	Kim, 2005	54.3	-	34,006	0.18
	Gopalakrishnan, 1969	29.	-	30,300	0.17
	Ladaoui, 2011	86.0	-	45,450	0.27
	Granger, 1996	43.5	-	38,600	0.21
	Roll, 1966	41.4	-	35,000	-
Mortar	Buffo-Lacarrière, 2011	26.5	2.3	24,600	0.20

concrete CII, compressive strength of 44.1 MPa in 8, concrete CIII, compressive strength of 54.3 MPa in 9). In these experiments,  $\epsilon_1$  was the strain in

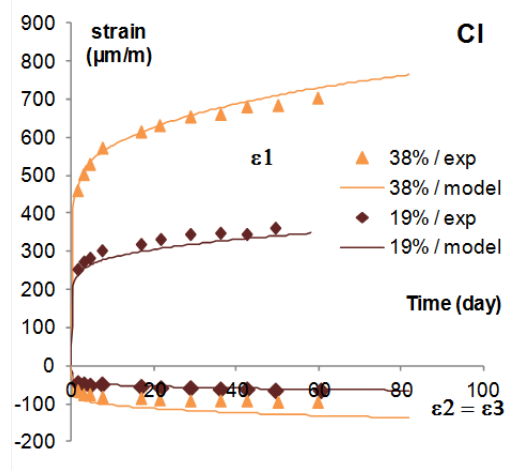


Figure 7: Kim test, Concrete CI, uniaxial compression, basic creep with instantaneous elastic strain for two loading levels (19 and 38%)

the loading direction and  $\epsilon_2$  and  $\epsilon_3$  were the transverse strains (in unloaded

Table 4: : Creep and shrinkage model parameters

Material reference	$\tau_{ref}^K$ Day	$\tau_{ref}^M$ Day	$\varepsilon_{ref}^M$ -	$\psi^K$ -	$M_{shr}$ MPa	$b$ -	$m_{vg}$ -
Kim, 2005, CI	2.	15.	10.e-5	4.	-	-	-
Kim, 2005, CII	2.	15.	9.e-5	4.	-	-	-
Kim, 2005, CIII	3.	20.	7.5e-5	4.	-	-	-
Gopalakrishnan, 1969	1.	10.	6.5e-5	4.8	-	-	-
Ladaoui, 2011	5.	10.	5.5e-5	5.	-	-	-
Granger, 1996	1.	12.	12.e-5	3.5	40.	0.5	0.5
Roll, 1964	1.	6.	12.e-5	4.5	28.5	0.5	0.5
Buffo-Lacarriere, 2011	2.	10.	18.e-5	4.	25.5	0.55	0.5

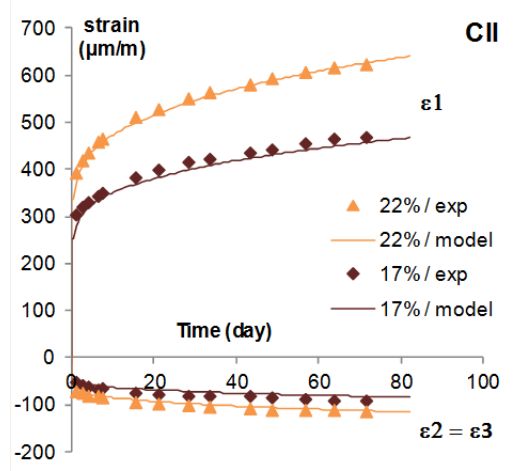


Figure 8: Kim test, Concrete CII, uniaxial compression, basic creep with instantaneous elastic strain for two loading levels (17 and 22%)

295 directions for uniaxial tests). Calculated values were obtained by calibrating the two characteristic times  $\tau_{ref}^K$  and  $\tau_{ref}^M$  and the characteristic creep strain  $\varepsilon_{ref}^M$  on the strains  $\varepsilon_1$  obtained for the lowest loading of each concrete (Table 4). In these experiments, the increase of strength was obtained by increasing the

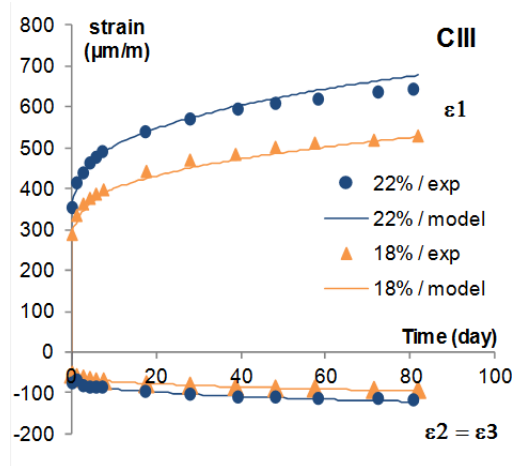


Figure 9: Kim test, Concrete CIII, uniaxial compression, basic creep with instantaneous elastic strain for two loading levels (18 and 22%)

cement content, and reducing W/C ratio, with constant aggregate content [16].

300 The model calibration gave the lowest characteristic creep strain  $\varepsilon_{ref}^M$  for the highest concrete strength. It is important to note that the model gives a good prediction of the strains in the unloaded directions with the calibration of parameters in the loading direction only. This is a consequence of the assumption presented in equation (1) where creep strain rates derive from elastic strains and

305 no supplementary fitting is necessary. In the same way, all the strains for the second loading were well-predicted without additional fitting. In these experiments, all the loadings were lower than 40% of the compression strength and the experimental results show the good agreement between measured strain and stress level.

### 310 3.2. Basic creep under multiaxial loadings

The aim of this part is to test the aptitude of model to reproduce the basic creep under multiaxial loading from experimental data presented in the literature: Gopalakrishnan (for loading and unloading conditions [15]) and Kim (only for loading conditions [16]).

315 *For loading conditions.* First, the model was tested on Kim's experiments, already presented in the previous part for uniaxial loading. The three concretes described in the previous part were subjected to bi and tri-axial loadings. The results of experimentation and modelling are reported in Figures 10, 11 and 12.

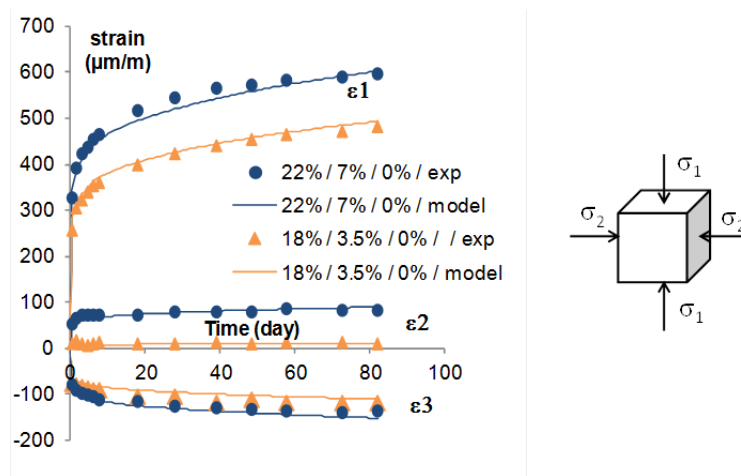


Figure 10: Kim's test, Concrete CIII, biaxial compression, with two loading levels (curves designation: loading levels in, respectively, directions 1 / 2 / and 3), basic creep with instantaneous elastic strain

320 For the calculations, the strains in the three directions were obtained with the parameters calibrated on the strain measured in the loaded direction of the uniaxial tests for the same concrete (shown above). This comparison shows that the model is able to predict strains in multiaxial conditions with only one measurement in a uniaxial test and without supplementary fitting (for five  
325 bi and tri-axial loadings). This result shows the interest of the developments presented in the first part of this paper, specifically the assumption concerning the proportionality between instantaneous creep velocity and current elastic strains (equations (1) and (18)), which is able to predict strains in a multiaxial loading from calibration on a uniaxial test, without supplementary parameters.

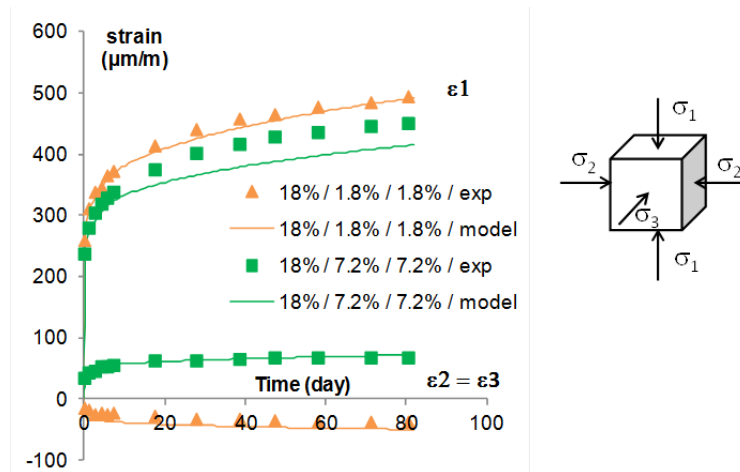


Figure 11: Kim's test, Concrete CIII, triaxial compression, with two loading levels (curves designation: loading levels in, respectively, directions 1 / 2 / and 3), basic creep with instantaneous elastic strain

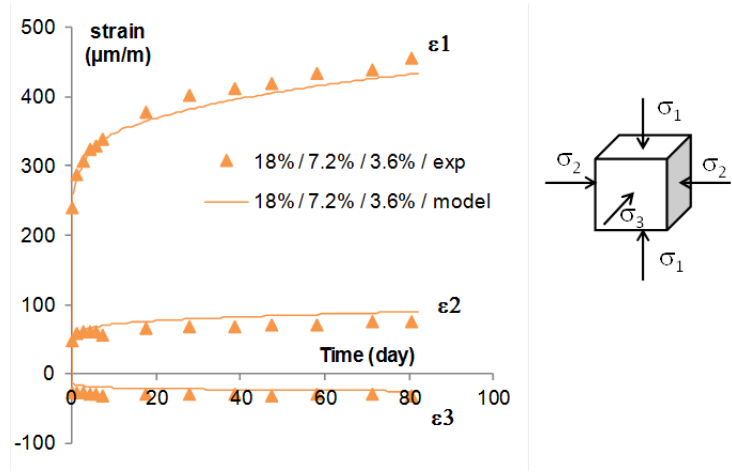


Figure 12: Kim's test, Concrete CIII, triaxial compression, with a same loading levels in the three directions, basic creep with instantaneous elastic strain

330 *With unloading.* During the life of a structure, stress on the concrete fluctuates. When the concrete is unloaded, creep recovery occurs. To be used in concrete structural modelling, the model has to be able to reproduce this phenomenon,

which is taken into account by the partition between reversible (Kelvin) and irreversible (Maxwell) modules. During Gopalakrishnan's experiments [15], different uni- and multi-axial tests were performed :

- uniaxial loading at 12.5 MPa for 28 days followed by unloading,
- biaxial loading at 12.5 and 7.2 MPa, respectively, in directions 1 and 2 for 28 days followed by unloading,
- triaxial loading at 13.5, 12.8 and 6.4 MPa, respectively, in directions 3, 2 and 1 for 63 days, then increase of the compressive stress to 13.4 MPa in the direction 1 (stresses were unchanged in the other two directions), then total unloading in the three directions at 94 days.

In this section, to facilitate interpretation of the graphics in multi-axial loading conditions, the strain sign has not be reversed. This unusual convention concerns only figures 13,14 and 15. As for Kim's tests, the model was calibrated on the uni-axial test only (Table 4 and Figure 13), and then it was used to predict creep deformation in the three directions of multi-axial loadings (Figures 14 and 15).

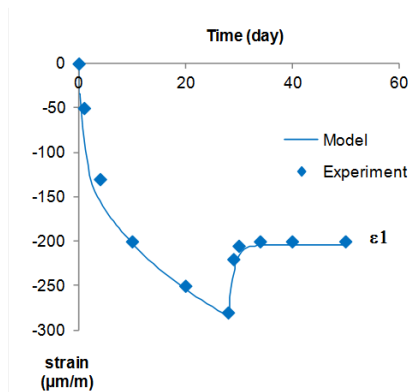


Figure 13: Gopalakrishnan's test, uniaxial compression, basic creep strain

The Young's modulus of concrete was not given in the Gopalakrishnan's paper [15]. It was assessed from the compressive strength with a usual standard relationship [43] linking compressive strength and Young's modulus. Also, tests

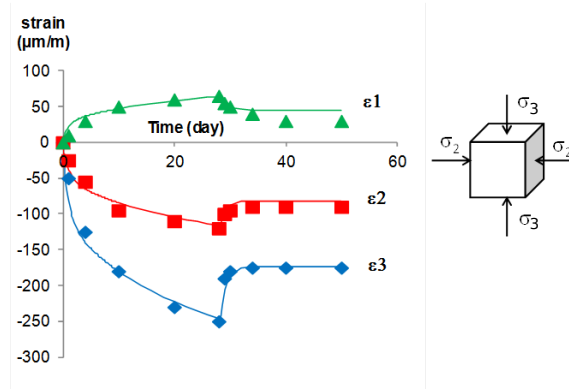


Figure 14: Gopalakrishnan’s test, biaxial compression, basic creep strain

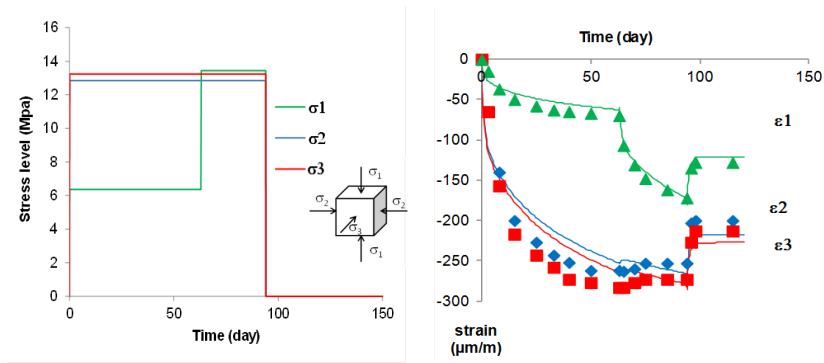


Figure 15: Gopalakrishnan’s test, triaxial compression, basic creep strain

were performed 8 days after casting, and the increase of the concrete Young’s modulus with hydration had to be taken into account to obtain a good reproduction of these tests. Here again, the standard kinetic law of the model code was used [43]. Calculations for the biaxial test (Figure 14) are in good agree-  
 355 ment with experiment for both the loading and recovery parts. For the triaxial test (Figure 15), the magnitude of creep deformations in the three directions was well-predicted by the model and the evolution of deformation with time was quite well-reproduced for the first loading, with a slight delay for the two directions with the largest loading (directions 2 and 3) while deformation calcu-

lated along direction 1 is in accordance with measurements. Small differences  
can be noted in the second part of test (between 63 and 94 days) where the  
model predicts a small negative slope while experiments show little evolution  
for these two directions. In this period, the concrete specimen was kept in an  
isotropic stress state. The measurements showed a stabilization of deformation  
in the two directions previously loaded at 13 MPa (2 and 3), while the deforma-  
tion rate increased in direction (1), for which stress increased from 6.4 to  
13.4 MPa. This test shows that concrete creep exists under isotropic loading  
but with different evolutions according to the direction previously loaded. Cal-  
culations showed the increase of deformation rate in the third direction, but  
only partially showed the stabilization in the other two directions. If creep  
modelling did not consider directional consolidation during creep phenomena,  
spherical creep would lead to identical creep rates in the three directions. Di-  
rections that have been previously subjected to higher loading (directions 2 and  
3) show a smaller creep rate than the direction with smaller loading (direction  
1) because directions 2 and 3 were already consolidated when the loading be-  
came isotropic. With the anisotropic consolidation, the present modelling takes  
this effect into consideration. Moreover, the Drucker-Prager criterion does not  
allow for non-linear creep under isotropic since the criterion cannot be reached  
in this condition. This leads to a decrease (on average) in the creep deformation  
velocity in isotropic conditions, in comparison with anisotropic loading, and ex-  
plains the difference of creep strain according to the multi-axial stress state: a  
creep strain of about  $300\mu m/m$  is obtained for the uni-axial loading (Figure 13)  
after 28 days of loading while in bi- (Figure 14) or tri- (Figure 15) axial loading  
the creep strain in the same direction, and for a same applied stress, is about  
 $250\mu m/m$ . The two original points of the model (anisotropic consolidation and  
creep non-linearity versus loading) are needed to obtain relevant modelling of  
creep in bi- and tri-axial stress conditions from model calibration on uni-axial  
loading.

### 3.3. Creep during hydration

Concrete creep velocity is higher at early age than for aged concrete. In the model, the phenomenon is a consequence of the dependence of creep rate on elastic strains, which depend on the instantaneous properties of concrete. As Young's modulus, strengths and equivalent capillary pressure depend on the hydration rate (23), instantaneous strains depend on the current values of these properties and, through equations 1 and 18, creep rates are changed. Consequently, creep rates are higher at early age. To test the ability of model to reproduce early age behaviour, autogenous shrinkage and creep a few days after casting were simulated. Experimental results were obtained with mortar specimens (see composition in Table 2). The specimens were placed in a climatic room ( $20^{\circ}\text{C} \pm 1^{\circ}\text{C}$ ) and protected from water exchanges. Shrinkage strains were recorded from 24 hours after casting. Creep tests used incremental loading (first loading 3 days after casting and reloading 7 and 69 days after casting). This incremental loading allowed the loading rate to be adapted to the progressive increase in the compressive strength (load equal to 30 % of  $R_c$ ). The loading and environmental conditions are summarized in Figure (16). The

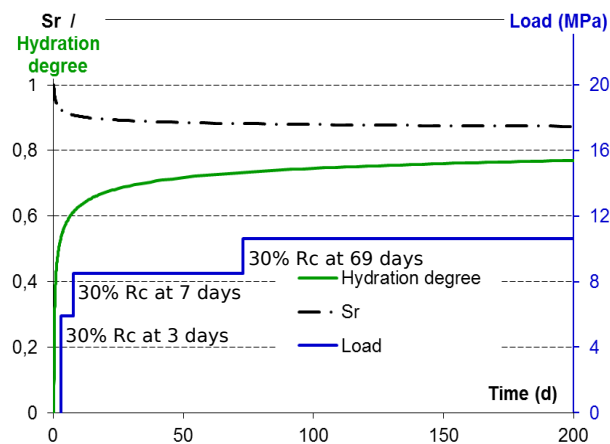


Figure 16: Buffo-Lacarrière's tests, loading kinetics at early age, hydration rate and water saturation rate (Sr)

405

hydration and saturation rates were computed using a multiphasic hydration model [35][44]. Hydration degree was used to determine the evolution of the mechanical properties of the concrete from the percolation threshold (0.31 for this mortar), using the de Schutter's laws (23), with a reference hydration rate ( $\xi_{ref}$  in Equation 23) of 0.7, corresponding to the mechanical characteristics at 28 days given in Table 3. The hydration model also computes the porosity and the water content which were used to calculate the saturation rate, inducing capillary pressure according to equation (22). Figure 17 compares the experi-

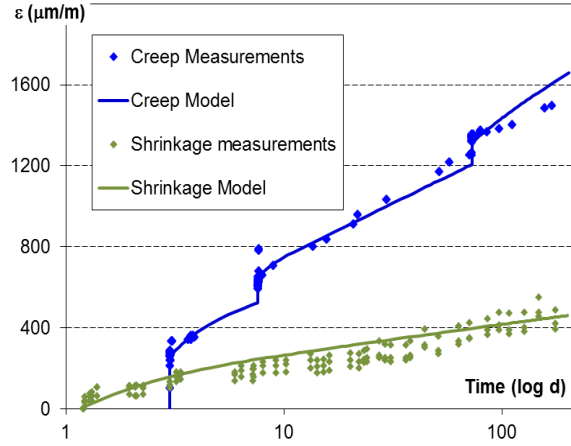


Figure 17: Buffo-Lacarriere's tests, total delayed strains of loaded specimen and free shrinkage simulations compared to experimental results

mental results and those obtained with the creep model for hardening concrete. The influence of internal variable updating (24) and of elastic parameters (23) according to the development of hydration was highlighted by simulating the same creep test with the creep parameters blocked at their value at 28 days, as illustrated by the dot-dash curve in figure 18. In this figure, the strain that would be obtained without creep is also presented (elastic strain corresponding to the dotted curve). This latter curve represents only the elastic strain induced by the mechanical loading and the elastic part of autogeneous shrinkage. The creep is the difference between the creep curve and this curve. It can be seen

that, with a loading at 3 days after casting corresponding to an hydration degree of 0.48, the real creep is approximately 20% greater than that computed without a hardening law. The difference would be greater if loading were performed earlier, whereas it is very close to the curve considering hardening effects. Despite this fitting on a three days old concrete, the model was able to extrapolate successfully the early age behaviour of a large instrumented structure studied during the CEOS.fr research project [38]. In this application vibrating wires sensors were embedded in the concrete to measure the mechanical strains since the very beginning of the hardening (a few hours after casting) until several months. Complementary tests should be performed to be sure that the model is applicable to other concrete types and loading chronologies. To this purpose, interesting tests performed at early age are available in the literature. Among others, tests used in [33], [45], [46] and [47] could also be simulated.

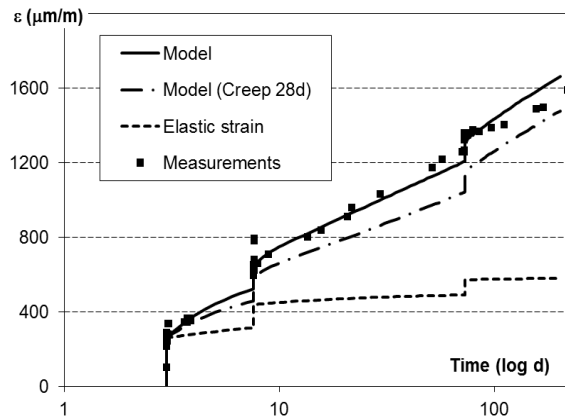


Figure 18: Buffo-LacARRIERE's tests, Creep and Shrinkage simulations with or without hydration effect : Model with hardening law (line), Model with creep blocked parameters corresponding to 28 days (dot-dash line), elastic strain (dotted line)

435

### 3.4. Creep in temperature

For calculations of structures for nuclear wastes disposal, particular attention was paid to creep in various temperature conditions. The capability of

the model to reproduce creep strains in different thermal conditions was tested  
 440 on Ladaoui's experiments [20] [21] on a high performance concrete (compressive strength  $86MPa$ , Young's modulus  $45,450MPa$ , see Table 3). After one year of curing, creep tests were performed under  $26MPa$  in atmospheres at  $20^{\circ}C$ ,  $50^{\circ}C$  and  $80^{\circ}C$  under autogenous conditions. The effect of temperature on creep strains is shown in Figure 19. In the model, this increasing effect  
 445 of temperature is explained by the decrease in water viscosity: the Arrhenius law acts on characteristic times  $\tau^K$  and  $\tau_{ij}^M$  through the activation energy of water viscosity (10), the increase of creep potential (11), and a 10% reduction of Young's modulus (measured by Ladaoui) induced by temperature damage [20]. These three effects have to be taken into account to reproduce the effect of temperature on concrete creep. To obtain the calculations presented in Fig-

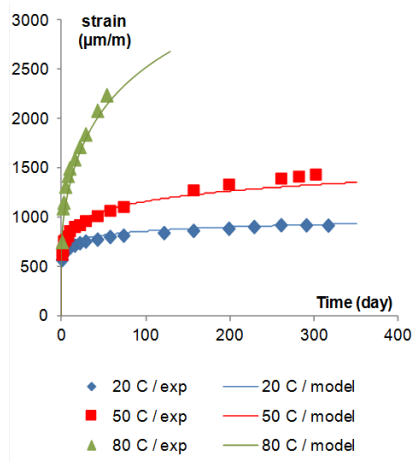


Figure 19: Ladaoui's tests, uniaxial compression at three different temperatures ( $20^{\circ}C$ ,  $50^{\circ}C$  and  $80^{\circ}C$ ), total delayed strain compared with experimental results

450

ure 19, Ladaoui's experimental results on basic creep at  $20^{\circ}C$  and  $50^{\circ}C$  were used to fit the activation energy affecting the creep potential ( $E_p^a$  in equation (11)). An energy close to  $23700J/Mol$  is necessary to reproduce the creep strains at  $20^{\circ}C$  and  $50^{\circ}C$  with the same parameter's set (Figure 19 and Table  
 455 4). Once the activation energy is fitted, the model can be used to predict the

creep at 80°C (creep strains four times higher at 80°C than at 50°C Figure  
 19). In consequence, only one set of parameters is necessary to perform calcula-  
 tions of loaded concrete submitted to various thermal conditions. As explained  
 above, fitting the activation energy for creep potential need experimentations  
 460 in temperature higher than  $T_{thr} \approx 45^\circ\text{C}$  (cf. equation (11)). According to [20],  
 this temperature must be exceeded to modify creep potential. If a creep test  
 is performed below  $T_{thr}$ , creep is accelerated only through the modification of  
 interstitial water viscosity. An interesting application could be to perform creep  
 tests at  $\approx 40^\circ\text{C}$  to obtain fast creep strains without changing the creep poten-  
 465 tial. The measurements at high temperature could then be analysed with the  
 model, using only the effect of temperature on water viscosity (equation (10))  
 to predict the behaviour of concrete in usual conditions.

### 3.5. Drying creep

The moisture conditions of concrete structures usually vary. The effect of  
 470 drying on concrete creep is well-known. Phenomena at the origin of concrete  
 creep are partly the same in endogenous and in drying conditions. The sup-  
 plementary strains obtained for drying creep are explained in the model by an  
 increase of shrinkage in loaded conditions, as proposed in [11] and [48]. Creep  
 modelling has to be able to reproduce basic and drying creep with the same  
 475 parameters for the rheological model. In order to obtain such a result, it has  
 been proposed to introduce the Equation (20). To calibrate the only param-  
 eter of this equation (called  $(\sigma_{dc})$  in Equation (20)), three measurements are  
 necessary: the basic creep, the drying shrinkage and the total creep. The abil-  
 ity of the model to obtain such results was tested on Granger's experiments  
 480 [41]. Granger measured the concrete basic creep, shrinkage and total creep, as  
 illustrated in Figure 20.

The concrete strength was  $43.5\text{MPa}$ , the Young's modulus  $38600\text{MPa}$ .  
 Specimens were loaded at  $12\text{MPa}$  (loading level of 27%). The relative humid-  
 ity for shrinkage and drying creep was 50%. The moisture transfer simulations  
 485 necessary to obtain relevant water concentration for drying shrinkage and total

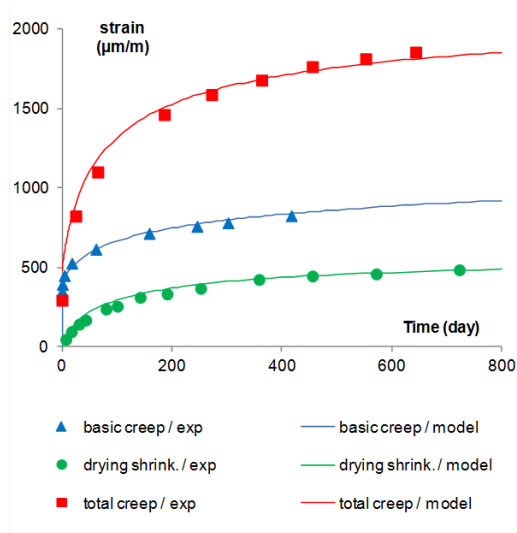


Figure 20: Granger's tests, drying shrinkage, total and basic creep with instantaneous elastic strain, comparison with experimental data

creep tests are presented in [11]. Mechanical calculations were then performed with the water saturation degrees obtained on the mesh for each time step by these calculations. The Biot coefficient ( $b$  in equation (21)) for this concrete was taken to 0.5 (not measured but this is a common value for concrete). The parameters of creep modelling were then calibrated to obtain the basic creep and the shrinkage modulus was fitted to obtain a good assessment of the measured shrinkage strains (Figure 20, Table 4 for the parameters). The total creep can be obtained with a parameter  $\sigma_{dc} = 18MPa$  (Figure 20). This means that a compression stress of  $18MPa$  is able to double the shrinkage (relative to a free shrinkage condition). Therefore, the model can reproduce creep strain in autogenous and drying conditions with the same parameters for the creep model.

### 3.6. Creep non-linearity

Finally, the model was used to analyse the creep non-linearity. Rolls experiments were employed for this purpose [13]. In 1964, Roll studied the effect of

the loading level on concrete creep in drying conditions. The same concrete was subjected to different loading levels ranging from 20% to 65% of the compressive strength. The compressive strength and the Young's modulus used for the simulation are given in Table 3. During the creep tests, specimens were kept in an atmosphere at 65% RH. The following calculations were performed with the concrete Young's modulus measured at 220 days (Table 3). It was also assumed that the saturation degree of concrete evolved from 100% to 65% between the loading date and 220 days in order to fit the shrinkage strains (Figure 21).

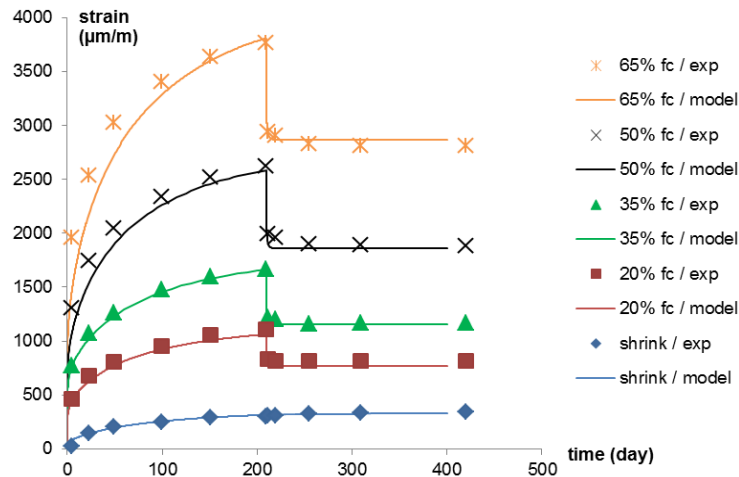


Figure 21: Roll's test, drying shrinkage and total creep with instantaneous elastic strain, comparison with experimental data

Once the shrinkage had been calibrated, the creep parameters of the model were fitted on the loading level of 35% which is a usual stress level for creep tests (Figure 21 Table 4 for the parameters). It was then possible to obtain the creep strain for the other three loading levels (20, 50 and 65%) during the loading phase and the recovery with no supplementary calibration (with the parameter  $\chi^M$  of equation (12) equal to 2). This application confirms that it is possible to reproduce the non-linearity of creep with increasing loading level by using only one parameter and the concept of a non-linear Maxwell module (non-

linear evolution of creep potential  $\varepsilon^M$  ) and without creep damage which would lead to an overestimation of elastic strains at unloading (due to the decrease of the Young's modulus by creep damage, as suggested in [49]).

#### 520 4. Conclusion

The model presented in this paper allows non-linear creep, multi-axial creep, and drying creep to be simulated in the framework of poro-mechanics. The non-linear creep can be a consequence of a stress transfer from viscous phases to non-viscous ones. This stress-transfer mechanism concentrates stresses on non-viscous phases in the long term, which can change the creep potential if the loading level is sufficient, otherwise the consolidation process prevails and creep slows. In addition, drying creep is interpreted as a modification of the transmission of capillary forces from micro-structure to the macro-scale. This modification depends, in the model, on the applied stress, which acts as a pre-stress delaying de-bonding between paste and aggregates in the direction of applied stress. Finally the non-linear creep and the modulation of capillary forces are coupled in the framework of poro-mechanics. The resulting model is a macroscopic one, implemented in a finite element code. It can be used for the simulation of structures subjected to high levels of loading and various moisture or temperature conditions. The studies selected in the literature and performed to test the model have highlighted several interesting aspects of creep. Among others, the following could have practical consequences:

- Confrontation of creep strain amplitudes in unloaded directions and loaded directions show that the ratios of creep strains in different directions are of the same magnitude as the ratios of elastic strains, so assuming creep velocity is proportional to elastic strains is a reliable and simple way to link creep velocity and loading conditions.
- A comparison of Roll's and Gopalakrishnan's tests shows that the non-linear dependence of the creep on strong loading can be based on a criterion

545 using the equivalent shear stress (Drucker Prager). It means, the non-linear part of the creep potential is related to the deviatoric part of stress tensor, with a minimizing effect of its isotropic part.

• Nevertheless, thanks to Gopalakrishnan's triaxial test, it has been shown that, in the case of spherical loading following a deviatoric loading, creep  
550 strains in the principal directions of stresses continue while the stress state becomes isotropic. The fact that creep strain remains anisotropic while the stress state is isotropic shows that consolidation is an anisotropic phenomenon.

• According to meso-scopic analysis of the consequences of paste shrinkage,  
555 drying creep can be interpreted as a modification of the hydric forces transmitted from paste to macroscopic level. This modelling allows the basic creep model and the capillary effects to be merged into a single poromechanical formulation. The advantages of doing this are multiple: first it reduces the number of model parameters compared to a serial model in  
560 which each phenomenon is modelled separately, and, more interestingly, automatically considers some coupling such as coupling between non-linear creep and shrinkage, multi-axial creep and shrinkage, or non-linear and multi-axial creep in temperature.

• In simulations of Roll's and Kim's tests, the fact of strain recovery after a  
565 creep test leads to a specimen stiffness equal to the initial stiffness (before the creep test) shows that damage induced by creep has no macroscopic effect on concrete stiffness, so the creep strain non-linearity with respect to loading highlighted in Roll's and Kim's tests must be modelled by a modification of creep potential without macroscopic damage.

570 Forthcoming stages intended to clarify the model will concern a better comprehension of temperature effects and equivalent water pressure effects in transient thermo-hydric conditions, which should improve the comprehension of temperature effect on equivalent capillary forces. An experimental set-up has been

developed at LMDC in Toulouse so that such tests can be carried out. Another  
575 subject of concern could be the possibility of using the creep model in tension.  
In fact, the present model assumes the basic phenomena involved in delayed  
strains are independent of the sign of the stress. This assumption is in accor-  
dance with some results but not confirmed by others. The authors think that  
the equivalent capillary pressure considered in the model could play a major  
580 role in the asymmetry of behaviour in some tests [50] [8] [51] [47], and this  
assumption would merit investigations by comparison with reliable tests.

To finish, it should be noted that the model applications presented in this  
paper were selected for their complementarity. They allow the models to be  
tested under very different environmental and loading conditions and hence  
585 constitute an interesting data set to benchmark creep models implemented in  
finite element codes.

### Acknowledgements

The authors thank the French Ministry of Research for its financial support  
through the national project CEOS.fr and the ANR projects MEFISTO, MO-  
590 SAIC and MACENA which contributed to the clarification of different parts of  
the model. Andra is also thanked for its scientific contribution and for fund-  
ing the tests . EDF-CIH and more specifically E.Bourdarot and E.Grimal are  
thanked for their scientific collaboration concerning the coupling of the creep  
model with internal swelling reaction models [40] [52].

### References

- 595 [1] Z. P. Bazant, A. Asghari, J. Schmidt, Experimental study of creep of hard-  
ened Portland cement paste at variable water content, *Matériaux et con-  
structions* 9 (52) (1995) 279–290.
- [2] F. J. Ulm, M. H. Jennings, J. M. P. Roland,  
600 *Mechanics and Physics of Creep, Shrinkage, and Durability of Concrete* (ASCE),

- in: F.-J. Ulm, J. M. Hamlin, J. P. Roland (Eds.), Ninth International Conference on Creep, Shrinkage, and Durability Mechanics (CONCREEP-9) Cambridge, Massachusetts, United States September 22-25, 2013, American Society of Civil Engineers, ISBN (print): 978-0-7844-1311-1, Boston, 2013.
- 605 URL <http://ascelibrary.org/doi/book/10.1061/9780784413111>
- [3] T. Tanabe, S. Ono, H. Morimoto, H. Nakamura, Y. Ishikawa, Development of Comprehensive Platform for the Estimation of Volume Change and Damage in Cement in: Mechanics and Physics of Creep, Shrinkage, and Durability of Concrete, American Society of Civil Engineers, 2013, pp. 412–420.
- 610 doi:doi:10.1061/9780784413111.049.  
URL <http://dx.doi.org/10.1061/9780784413111.049>
- [4] C. a. Jones, Z. C. Grasley, Short-term creep of cement paste during nanoindentation, Cement and Concrete Composites 33 (1) (2011) 12–18.
- 615 doi:10.1016/j.cemconcomp.2010.09.016.  
URL <http://linkinghub.elsevier.com/retrieve/pii/S0958946510001460>
- [5] Z. P. Bažant, S. Prasannan, Solidification theory for concrete creep: I. Formulation, Journal of Engineering ... 115 (8) (1989) 1691–1703.
- [6] F. Wittmann, P. Roelfstra, H. Mihashi, Y. Huang, X. Zhang, N. Nomura, Influence of age of loading, water-cement ratio and rate of loading on fracture energy of concrete, Materials and Structures 20 (2) (1987) 103–110.
- 620 doi:10.1007/BF02472745.  
URL <http://www.springerlink.com/content/7647512012255515/>
- [7] F. Beltzung, F. H. Wittmann, Role of disjoining pressure in cement based materials, Cement and Concrete Research 35 (12) (2005) 2364–2370.
- 625 doi:10.1016/j.cemconres.2005.04.004.  
URL <http://linkinghub.elsevier.com/retrieve/pii/S000888460500102X>
- [8] P. Rossi, J.-L. Tailhan, F. Le Maou, L. Gaillet, E. Martin, Basic creep behavior of concretes investigation of the physical mechanisms by using acoustic emission

- 630 Cement and Concrete Research 42 (1) (2012) 61–73.  
doi:10.1016/j.cemconres.2011.07.011.  
URL <http://linkinghub.elsevier.com/retrieve/pii/S0008884611002110>
- [9] H. Jennings, E. Masoero, M. Pinson, E. Strekalova, P. Bonnaud, H. Manzano, Q. Ji, J. Thomas, R. Pellenq, F. Ulm, M. Bazant, K. Van Vliet,  
635 Water Isotherms, Shrinkage and Creep of Cement Paste: Hypotheses, Models and Experiments,  
in: Mechanics and Physics of Creep, Shrinkage, and Durability of Concrete, American Society of Civil Engineers, 2013, pp. 134–141.  
doi:doi:10.1061/9780784413111.015.  
URL <http://dx.doi.org/10.1061/9780784413111.015>
- 640 [10] S. Grasberger, G. Meschke, Thermo-hygro-mechanical degradation of concrete: From coupled 3D mat  
Materials and Structures 37 (4) (2004) 244–256.  
doi:10.1007/BF02480633.  
URL <http://www.springerlink.com/index/10.1007/BF02480633>
- [11] A. Sellier, L. Buffo-Lacarrière, Towards a simple and unified modelling of  
645 basic creep, shrinkage and drying creep of concrete, European Journal of  
Environmental and Civil Engineering 13 (10) (2009) 1161–1182.
- [12] R. Sierra, Contribution to the study of hydraulic calcium silicate, Tech.  
Rep. 39, Institut Francais des Sciences et Technologies des Transports,  
de l’Amenagement et des Reseaux (IFSTTAR) 14-20 bd Newton, Cité  
650 Descartes, Champs su Marne 77447 Marne la Vallée Cedex 2 France, Marne  
la vallée (1974).  
URL <http://trid.trb.org/view.aspx?id=1068256>
- [13] F. Roll, Long Time Creep-Recovery of Highly Stressed Concrete Cylinders,  
in: ACI SP9 Symposium on creep, Portland Cement Association, Detroit,  
655 1964, pp. 115–128.
- [14] S.-T. Gu, B. Bary, Q.-C. He, M.-Q. Thai,  
Multiscale poro-creep model for cement-based materials, International

- Journal for Numerical and Analytical Methods in Geomechanics 36 (18)  
 (2012) 1932–1953. doi:10.1002/nag.1080.  
 URL <http://dx.doi.org/10.1002/nag.1080>
- 660 [15] K. S. Gopalakrishnan, A. M. Neville, A. Ghali, Creep Poisson's Ratio of  
 Concrete Under Multiaxial Compression, ACI Journal proceedings 66 (12)  
 (1969) 1008–1019.
- [16] S. Y. Kim, J. K. Kim, Y. Y. Kim, S. H. Kwon,  
 665 Experimental studies on creep of sealed concrete under multiaxial stresses,  
 Magazine of Concrete Research 57 (10) (2005) 623–634.  
 doi:10.1680/macr.2005.57.10.623.  
 URL <http://www.icevirtuallibrary.com/content/article/10.1680/macr.2005.57.10.623>
- [17] A. Sellier, L. Buffo-Lacarrière, S. Multon, T. Vidal, X. Bourbon, Nonlinear  
 670 basic creep and drying creep modelling, in: Rossi & Tailhan (Ed.), SSCS  
 conference, Aix en Provence, 2012.
- [18] M. Vandamme, Q. Zhang, F. Ulm, R. Le  
 Roy, B. Zuber, E. Gartner, P. Termkhajornkit,  
 Creep Properties of Cementitious Materials from Indentation Testing: Significance, Influence of Relat  
 675 in: Mechanics and Physics of Creep, Shrinkage, and Durability of  
 Concrete, American Society of Civil Engineers, 2013, pp. 48–61.  
 doi:doi:10.1061/9780784413111.005.  
 URL <http://dx.doi.org/10.1061/9780784413111.005>
- [19] F. Benboudjema, F. Meftah, J. Torrenti,  
 680 Interaction between drying, shrinkage, creep and cracking phenomena in concrete,  
 Engineering Structures 27 (2) (2005) 239–250.  
 doi:10.1016/j.engstruct.2004.09.012.  
 URL <http://www.sciencedirect.com/science/article/pii/S0141029604003359>
- [20] W. Ladaoui, T. Vidal, A. Sellier, X. Bourbon,  
 685 Analysis of interactions between damage and basic creep of HPC and HPFRC heated between 20 and

Materials and Structures 46 (2013) 13–23.

doi:10.1617/s11527-012-9879-1.

URL <http://www.springerlink.com/content/r772214181531482/http://www.springerlink.com>

- [21] T. Vidal, A. Sellier, W. Ladaoui, X. Bourbon,  
690 Effect of Temperature on the Basic Creep of High-Performance Concretes Heated between 20 and 80  
Journal of Materials in Civil Engineering (2014)  
B4014002doi:10.1061/(ASCE)MT.1943-5533.0001063.  
URL [http://dx.doi.org/10.1061/\(ASCE\)MT.1943-5533.0001063](http://dx.doi.org/10.1061/(ASCE)MT.1943-5533.0001063)

- [22] W. Ladaoui, T. Vidal, A. Sellier, X. Bourbon,  
695 Effect of a temperature change from 20 to 50C on the basic creep of HPC and HPFRC,  
Materials and Structures 44 (9) (2011) 1629–1639.  
doi:10.1617/s11527-011-9723-z.  
URL <http://www.springerlink.com/index/10.1617/s11527-011-9723-z>

- [23] D. C. Drucker, W. Prager, Soil mechanics and plastic analysis for limit  
700 design, Quarterly of Applied Mathematics 10 (2) (1952) 157–165.

- [24] M. Matallah, C. La Borderie, Inelasticity-damage-based model for numer-  
ical modeling of concrete cracking, Engineering fracture mechanics 76 (8)  
(2009) 1087–1108.

- [25] F. Bourgeois, N. Burlion, J. F. Shao,  
705 Modelling of elastoplastic damage in concrete due to desiccation shrinkage,  
International Journal for Numerical and Analytical Methods in Geome-  
chanics 26 (8) (2002) 759–774. doi:10.1002/nag.221.  
URL <http://doi.wiley.com/10.1002/nag.221>

- [26] N. S. Ottosen, Theoretical framework for modelling the behaviour of frictional materials,  
710 International Journal of Solids and Structures 22 (11) (1986) 1325–1342.  
doi:10.1016/0020-7683(86)90084-3.  
URL <http://www.sciencedirect.com/science/article/pii/0020768386900843>

- [27] M. Ortiz, A constitutive theory for the inelastic behavior of concrete, *Mechanics of Materials* 4 (1985) 67–93.
- 715 [28] O. Coussy, *Mechanics of Porous Continua*, 2nd Edition, 1995.
- [29] T. Rougelot, N. Burlion, D. Bernard, F. Skoczylas, About microcracking due to leaching in cementitious composites: X-ray microtomography description *Cement and Concrete Research* 40 (2) (2010) 271–283.  
doi:10.1016/j.cemconres.2009.09.021.  
720 URL <http://www.sciencedirect.com/science/article/pii/S0008884609002749>
- [30] H. W. Reinhardt, T. Wüstholtz, Stress induced shrinkage of concrete in tension, in: *Creep, Shrinkage and Durability Mechanics of Concrete and Concrete Structures*, Two Volume Set: Proceedings of the CONCREEP 8 conference held in Ise-Shima, Japan, 30 September-2 October 2008, CRC Press, 2008, p. 65.  
725
- [31] T. M. Van Genuchten, D. Nielsen, On describing and predicting the hydraulic properties of unsaturated soils, *Annales physicae* 3 (5) (1985) 615–628.
- [32] V. Baroghel-Bouny, M. Mainguy, T. Lassabatere, O. Coussy, Characterization and identification of equilibrium and transfer moisture properties for ordinary and high strength concrete *Cement and Concrete Research* 29 (8) (1999) 1225–1238.  
730 doi:10.1016/S0008-8846(99)00102-7.  
URL <http://linkinghub.elsevier.com/retrieve/pii/S0008884699001027>
- [33] G. D. Schutter, L. Taerwe, Degree of hydration-based description of mechanical properties of early aged concrete *Materials and Structures* 29 (6) (1996) 335–344.  
735 doi:10.1007/BF02486341.  
URL <http://www.springerlink.com/index/b700921468822716.pdf>
- [34] J. Torrenti, F. Benboudjema, Mechanical threshold of cementitious materials at early age, *Materials and structures* 38 (3) (2005) 299–304.  
740 URL <http://www.springerlink.com/index/L541212523167662.pdf>

- [35] L. Buffo-Lacarrière, A. Sellier, A. Turatsinze, G. Escadeillas, Finite element modelling of hardening concrete: application to the prediction of early age cracking for Materials and Structures 44 (10) (2011) 1821–1835. doi:10.1617/s11527-011-9740-y.  
745 URL <http://www.springerlink.com/index/10.1617/s11527-011-9740-y>
- [36] L. Buffo-Lacarriere, A. Sellier, Chemo-mechanical modelling requirements for the assessment of concrete structure service life, Journal of Engineering Mechanics (ASCE) 37 (9) (2011) 625–633.
- [37] A. Sellier, E. Bourdarot, S. Multon, M. Cyr, E. Grimal, Combination of structural monitoring and laboratory tests for the assessment of AAR-swelling: application to a gate structure dam, ACI Materials Journal 750 106 (3) (2009) 281–290.
- [38] L. Buffo-Lacarrière, A. Sellier, B. Kolani, Application of thermo-hydro-chemo-mechanical model for early age behaviour of concrete to experim  
755 European Journal of Environmental and Civil Engineering (2014) 1–14doi:10.1080/19648189.2014.896754.  
URL <http://dx.doi.org/10.1080/19648189.2014.896754>
- [39] P. Verpeaux, A. Millard, T. Charras, A. Combescure, A modern approach of large computer codes for structural analysis, in: Hadjian (Ed.), Proc-SMiRT, AASMiRT, Los Angeles, 1989, pp. 75–78.  
760
- [40] E. Grimal, A. Sellier, Y. Le Pape, E. Bourdarot, Creep, Shrinkage, and Anisotropic Damage in Alkali-Aggregate Reaction Swelling Mechanism-Part I: ACI Materials Journal-American Concrete Institute 105 (3) (2008) 227–235. doi:10.14359/19818.  
765 URL <http://www.concrete.org/publications/acimaterialsjournal/acijournalsearch.aspx?m>
- [41] L. Granger, Comportement différé du béton dans les enceintes de centrales nucléaires: analyse et modélisation, Ph.D. thesis, Ecole Nationale des Ponts et Chaussées, Marne-La-Vallée, France (1996).

- [42] L. Lacarrière, Prévission et évaluation de la fissuration précoce des ouvrages en béton,  
770 Ph.D. thesis (2007).  
URL <http://eprint.insa-toulouse.fr/archive/00000165/>
- [43] Code Model special activity group, Model Code 2010, Tech. Rep. September, fib, CEB-FIP (2011).
- [44] B. Kolani, L. Buffo-Lacarrière, A. Sellier, G. Escadeillas,  
775 L. Boutillon, L. Linger, Hydration of slag-blended cements, Cement and Concrete Composites 34 (9) (2012) 1009–1018.  
doi:10.1016/j.cemconcomp.2012.05.007.  
URL <http://dx.doi.org/10.1016/j.cemconcomp.2012.05.007><http://linkinghub.elsevier.com>
- [45] M. Cervera, J. Oliver, T. Prato, Simulation of construction of RCC dams. I: temperature and aging,  
780 Journal of Structural Engineering 126 (May 2010) (2000) 1053.  
URL <http://link.aip.org/link/?JSENDH/126/1053/1>
- [46] F. Benboudjema, J. Torrenti, Early-age behaviour of concrete nuclear containments,  
Nuclear Engineering and Design 238 (10) (2008) 2495–2506.  
doi:10.1016/j.nucengdes.2008.04.009.  
785 URL <http://linkinghub.elsevier.com/retrieve/pii/S0029549308002185>
- [47] M. Briffaut, F. Benboudjema, J. M. Torrenti, G. Nahas,  
Numerical analysis of the thermal active restrained shrinkage ring test to study the early age behavior  
Engineering Structures 33 (4) (2011) 1390–1401.  
URL <http://www.sciencedirect.com/science/article/pii/S0141029611000137>
- [48] P. Rossi, J.-L. Tailhan, F. Le Maou, L. Gaillet, E. Martin,  
790 Basic creep behavior of concretes investigation of the physical mechanisms by using acoustic emission  
Cement and Concrete Research 42 (1) (2011) 73–61.  
doi:10.1016/j.cemconres.2011.07.011.  
URL <http://dx.doi.org/10.1016/j.cemconres.2011.07.011>
- [49] C. Mazzotti, M. Savoia, Nonlinear Creep Damage Model for Concrete under  
795

Uniaxial Compression, *Journal of Engineering Mechanics* 129 (9) (2003)  
1065–1075.

[50] N. Ranaivomanana, S. Multon, A. Turatsinze,  
Tensile, compressive and flexural basic creep of concrete at different stress levels,  
800 *Cement and Concrete Research* 52 (2013) 1–10.  
doi:10.1016/j.cemconres.2013.05.001.  
URL <http://www.sciencedirect.com/science/article/pii/S0008884613001063>

[51] A. Hilaire, F. Benboudjema, A. Darquennes, Y. Berthaud, G. Nahas,  
Modeling basic creep in concrete at early-age under compressive and tensile loading,  
805 *Nuclear Engineering and Design* 269 (2014) 222–230.  
doi:10.1016/j.nucengdes.2013.08.034.  
URL <http://www.sciencedirect.com/science/article/pii/S002954931300383X><http://linking>

[52] E. Grimal, A. Sellier, Y. Le Pape, E. Bourdarot,  
Creep, Shrinkage, and Anisotropic Damage in Alkali-Aggregate Reaction Swelling Mechanism-Part II  
810 *ACI Materials Journal* 105 No 3 (2008) 236–242. doi:10.14359/19819.  
URL <http://www.concrete.org/publications/acimaterialsjournal/acijournalsearch.aspx?m>